Program Digest, 2019 IEEE International Ultrasonics Symposium (IUS)
Glasgow, Scotland, October 6-9, 2019

Microbubble-mediated erosion and monitoring for the therapeutic treatment of urinary stones

David G. Bell[1], Matthew A. Hopcroft[1], Yuri A. Pishchalnikov[1],
Daniel J. Laser[1], William M. Behnke-Parks[1]
[1]Applaud Medical, San Francisco, CA

***Abstract*— We report on engineered microbubbles designed to accumulate on surfaces of urinary stone and facilitate stone comminution through mechanical effects including inertial collapse and pressure focusing against the urinary stone surface. In one current application of these engineered microbubbles, small quantities of engineered microbubbles, suspended in an aqueous solution, are placed in the patient's upper urinary tract via a cystoscopically positioned catheter and energized by quasi-collimated beams of acoustic energy emanating from a treatment head positioned on the patient's lower back, with the peak pressures of the beam in the range of diagnostic ultrasound. Non-invasive acoustic monitoring of microbubble dynamics and correlating signatures of inertial collapse with treatment parameters presents a promising strategy for gaining further insights on the mechanism of action as well as intra-treatment monitoring for improving clinical outcomes. To explore this detection strategy, we seek to compare the change in mass loss of model stones and the inertial collapse of the microbubbles measured via acoustic spectroscopy as a function of time and pressure.**

Keywords—inertial cavitation, microbubble, ultrasound, urinary stones, lithotripsy

I. Introduction

Microbubble-enhanced lithotripsy is a novel treatment modality currently in clinical trials for urinary stone disease which leverages the accumulation of cavitation-nuclei onto biomineralizations to facilitate the erosion, pitting, and fragmentation of surfaces with acoustic insonation [1]. Cavitation nuclei, in the form of engineered microbubbles, expand and collapse against a solid surface in response to an acoustic wave, refocusing the acoustic driving pressure by two-to-three orders of magnitude [2,3]. Understanding the collective behavior of engineered microbubbles under treatment conditions will aid the optimization of treatment parameters and the development of intra-treatment monitoring and feedback.

Microbubble-enhanced lithotripsy consists of two interwoven temporal cycles (Fig. 1): a macrocycle of iterative placement of engineered microbubbles in proximity to a biomineralization (duration η) followed by acoustic insonation (duration ξ), with a nested microcycle within the insonation period to achieve a desired duty cycle.

To investigate the collective dynamics of engineered microbubbles on the macrocycle timescale, we have combined near-real-time mass-loss measurements of synthetic calculi with acoustic spectroscopy. Specifically, both the temporal and pressure dependencies of stone erosion were compared with signatures for inertial cavitation (*IC*) [4].

We found the temporal profile of the *IC* signal to be multiphasic with an initial burst followed by a long-lived tail. In contrast, the mass-loss rate $\dot{m}$ showed a stronger dependence pressure, but also displayed a trend towards higher proportional mass loss rate at shorter timescales consistent with the *IC* temporal profile. We conclude that the *IC* metric provides a quantitative assessment for microbubble presence and activity, whereas the *IC* temporal profile qualitatively follows the mass loss $\dot{m}$.

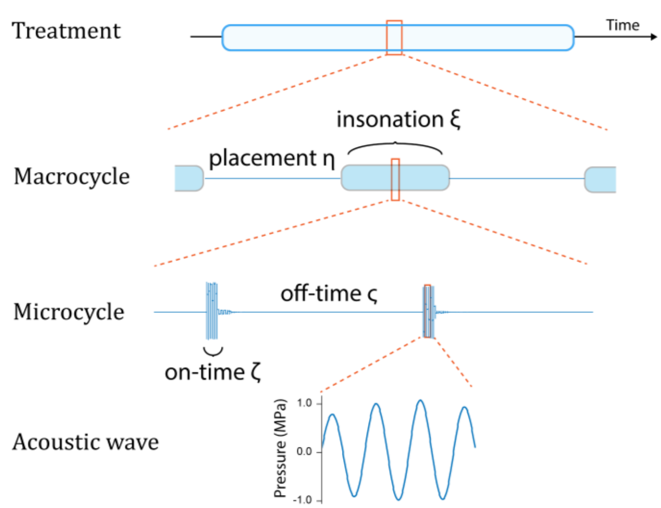

Fig. 1. The overall treatment (top) includes sequential iterations of macrocycles of microbubble placement (duration η) followed by acoustic insonation (duration ξ). The insonation period ξ comprises repeating microcycles of on-time (duration ζ) at a given pulse repetition rate (PRF) with associated off-time (duration ς). The on-time ζ consists of a sinusoidal acoustic wave with frequency f and corresponding to microsecond-long oscillations in pressure (bottom). In this study, we focused on the collective behavior of engineered microbubbles in response to the parameters of the macrocycle.

II. Materials and Methods

A. *Measurement of the rate of mass loss $\dot{m}$*

To measure the rate of mass loss $\dot{m}$ in near-real-time we developed an apparatus described in Ref. [5]. In brief, a low-drift differential load cell apparatus measured the buoyant mass of a submerged synthetic calculi after ultrasonic insonation in the presence or absence of engineered microbubbles. Insonation was achieved via a quasi-collimated beam (-3 dB region from 5 cm to 15 cm along the acoustic axis, beam width = 3.2 cm at a position 10 cm from the transducer face, f = 500 kHz). This wide-diameter beam applies a near-uniform pressure field (Fig. 2) on the surface of the target as measured by a spatial plot of pressure via calibrated hydrophone (HNR-0500, Onda Corp., Sunnyvale, CA). For macrocycle experiments we used an on-time ζ of 0.5 ms and an off time ς of 9.5 ms, corresponding to a pulse repetition rate (PRF) of 100 Hz. Synthetic calculi approximately 5 mm in diameter were made via extrusion with a composition of 55% hydroxyapatite, 20% Al_2O_3, and 25% microcrystalline cellulose binder (Riogen, Inc., Mullica Hill, NJ).

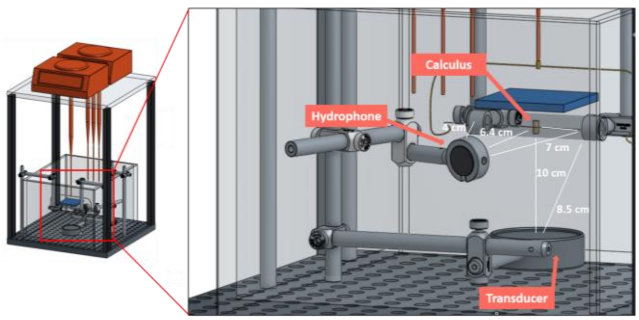

Fig. 2. Experimental set-up, consisting of a dual-load-cell measurement of submerged mass combined with a focused hydrophone (Sonic Concepts, Y107) aimed at the proximal surface of the stone (~70 degrees relative to the acoustic axis of the transducer). The blue square is acoustically absorbent material (F27 Precision Acoustics).

B. *Engineered microbubbles*

Engineered microbubbles [2,3] with concentration of 5e8 mL^{-1} were placed in proximity to the synthetic stone inside a model ureter (dialysis tubing, Carolina Biological Supply Company, Burlington, NC) via a 5F catheter (Cook Medical, Bloomington, IN) for period η of 30 seconds prior to each insonation period ξ. Shorter placement periods did not affect $\dot{m}$ (data not shown). During each insonation period, the first 5 to 15 seconds of acoustic signals were recorded.

C. *Measurement of acoustic spectra*

Acoustic traces were collected with a focused hydrophone (Y107, Sonic Concepts, Inc., Bothell, WA) placed 64 mm from the proximal surface of the synthetic calculi (Fig. 2). The hydrophone signals were amplified (Stanford Research Systems, SIM983, -3dB at 2 MHz) and recorded using the segmented memory settings of a LeCroy oscilloscope (HDO4024 Teledyne, LeCroy Corp., NY). The recorded

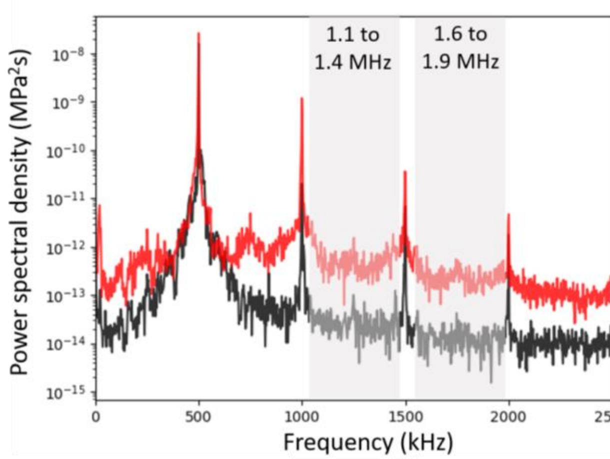

Fig. 3. Power spectral density (PSD) of the acoustic measurements with (red) and without (black) microbubbles. The fundamental frequency of insonation was f_0 =500 kHz. Spectral analysis of acoustic measurements was performed by summing the PSD over two bandwidth from 1.1 to 1.4 and from 1.6 to 1.9 MHz (grey), giving the metric for IC.

waveforms were processed using the Fast Fourier Transform (FFT) algorithm to find the power spectral density (PSD):

$$\mathrm{PSD}(f) = \frac{\Delta t}{N}\,|f \cdot \mathrm{FFT}(p(t))|^2$$

To exclude the harmonic at 1.5 MHz (Fig. 3), the PSD was integrated from 1.1 MHz to 1.4 MHz and from 1.6 MHz to 1.9 MHz; finally, the two integrands were summed to produce the inertial cavitation metric *IC*.

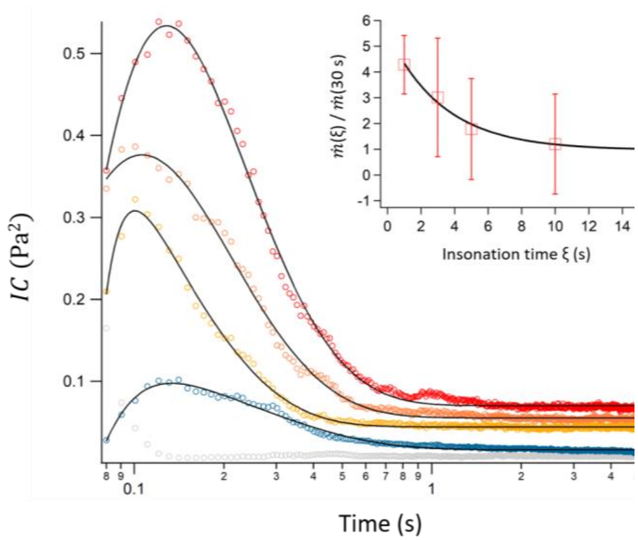

Fig. 4. The mean IC (n=9 to n=10) temporal profile reveals a long-lived tail at various applied pressures (red = 1.21 MPa, orange=1.06 MPa, yellow= 0.7 MPa, blue =0.43 MPa). IC temporal waveforms were fit to a double exponential model (black lines). The inset shows the rate of mass loss $\dot{m}$ for different insonation periods ξ (n=4 to n=9) normalized to the rate of mass loss during ξ = 30 seconds, and fitted to a single exponential (black line).

III. RESULTS

A. Collection of IC data

The *IC* data collected as a function of time from successive experiments were averaged (N=9 to N=10) and fit to a double exponential model of the form $IC = y_0+A_1e^{-t/\tau 1}+A_2e^{-t/\tau 2}$ (Fig. 4 and Table 1) for each applied pressure.

TABLE 1. Fitting coefficients to *IC* temporal profiles modeled as $IC=y_0+A_1e^{-t/\tau 1}+A_2e^{-t/\tau 2}$ (black curves in Fig. 4, errors in the fits < 10%)

	Applied Pressure			
	0.43 MPa	***0.7 MPa***	***1.06 MPa***	***1.21 MPa***
y_0 (Pa^2)	0.016	0.044	0.055	0.070
A_1(Pa^2)	-0.10	-0.20	-0.22	-0.54
τ_1 (s^{-1})	0.021	0.011	0.035	0.036
A_2 (Pa^2)	0.11	0.36	0.51	0.83
τ_2 (s^{-1})	0.23	0.10	0.14	0.15

B. Measurement of the rate of mass-loss versus time

Measurements of $\dot{m}$ require the absence of radiation forces, limiting measurements to the period after insonation ξ ceased. Therefore, to measure $\dot{m}$ for a given set of macrocycle parameters, the cumulative $\dot{m}$ distribution was measured for different values of ξ. $\dot{m}$ was measured for 4 different stones with each stone receiving a control condition of η = 30 seconds and ξ = 30 seconds, followed by the experimental condition: η = 30 seconds followed by ξ = 1, 3, 5 or 10 seconds (N=5). $\dot{m}$ for a given ξ was then normalized by time and the preceding measured erosion rate for ξ = 30 seconds: $(30/\xi)(\dot{m}(x)/\dot{m}(30s))$. The resulting normalized $\dot{m}$ are plotted in Figure 4, inset. Fitting a single exponential of the form $\dot{m} = Ae^{-(t/\tau)}$ produces a rate of change in $\dot{m}$ of τ = 3.3 seconds ± 0.3 seconds (A = 3.3732 ± 0.252 mg/min., τ = 3.3071 ± 0.581 seconds).

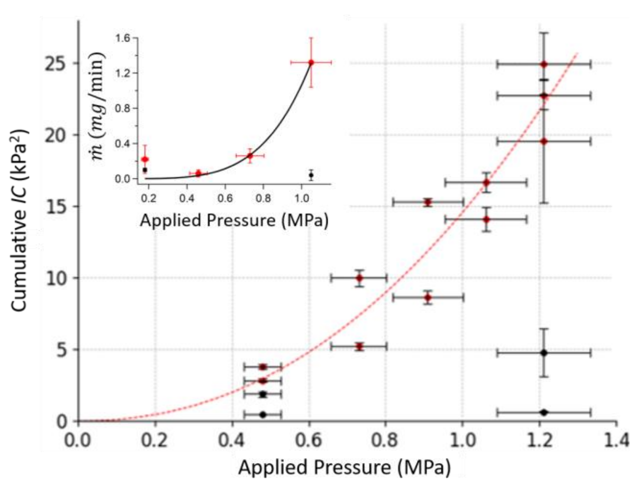

Fig. 5. The cumulative IC in the presence (red dots) or absence (black dots) of engineered microbubbles is plotted versus applied pressure. Fitting the IC signature from engineered microbubbles to a power law of the form Ax^α (red dotted line) consistent with the expected quadratic dependence (α = 2.17 (R2 ~ 0.9)). $\dot{m}$ showed a more complex dependence on applied pressure (inset). Fitting to a power law $y = Ax^\alpha$, results in a fit A = 1.066 ± 0.14, α = 4.37 ± 1.56 (error bars represent uncertainty in hydrophone calibration).

C. Measurement of the rate of mass-loss versus pressure

To compare $\dot{m}$ with *IC* as a function of applied pressure, $\dot{m}$ measurements were collected while varying the applied pressure. The rate of mass loss $\dot{m}$ measured as a function of applied pressure was fit to a power law of the form $y = AX^\alpha$, with a resulting fit of A = 1.0657 ± 0.136, and α = 4.37 ± 1.56. Given that each temporal profile versus pressure had similar time constants (Table 1), the cumulative amplitude of the *IC* time profile was then plotted versus applied pressure, and the resulting dependence (Fig. 5) was fit to a power law of the form AX^α; the data was best fit by the parameters A = 14.5, α = 2.17 (R = 0.9), consistent with a quadratic dependence.

IV. DISCUSSION

The measurement of inertial cavitation via analysis of acoustic spectra has been previously investigated experimentally [4, 8-11] as well as theoretically [12]. In brief, when the microbubble is driven far from equilibrium, during the final stages of collapse the microbubble rapidly shrinks, radiating an acoustic pulse. In the Rayleigh-Plesset type of equation, this radiated pressure *P* is proportional to the second derivative of the bubble volume *V*:

$$P = \frac{\rho_L}{4\pi r}\frac{d^2V}{dt^2}$$

where r is the radial distance from the center of the bubble, [6]. The broadband spectrum of these pressure pulses is distinct from the spectrum of the driving acosutic wave, and therefore provides a relative measurement of inertial cavitation [4].

Here we have characterized the relationships of inertial cavitation *IC* and rate of mass loss $\dot{m}$ on applied pressure and insonation time ξ. The rate of mass loss $\dot{m}$ displayed a more complex dependence on applied pressure, consistent with the non-linear fracture mechanics of materials as a function of pressure [7].

We observed that microbubble-mediated $\dot{m}(\xi)$ decays as a function of insonation time ξ on the ~second timescale. Although the temporal profile of *IC* displayed a complex sequence of events, the majority of the signal was distributed to the initial second timescale. We speculate that this decay in $\dot{m}$ could be due to the break-down in the mechanical structure of engineered microbubbles from processes such as merging, dissolution, or dislocation.

The temporal profile of *IC* suggests inertial cavitation of our engineered microbubbles, collectively, persists for tens of thousands of mechanical cycles, which is far larger than the previously observed threshold for fragmentation [4]. This, combined with the $\dot{m}$~second timescale, suggests an insonation time (ξ) on the second-timescale can be effective, making microbubble-enhanced lithotripsy an attractive technique for the treatment of biomineralizations.

In summary, we found *IC* to be a useful tool for monitoring the placement and pressure-driven inertial collapse of engineered microbubbles. The absence of engineered microbubbles produced two orders of magnitude lower *IC* relative to the placement of engineered microbubbles, and the *IC* signal showed the expected quadratic dependence on pressure. While the relative contribution of both applied pressure and the placement of microbubbles is difficult to decouple by acoustic spectroscopy alone, we note that when combined with other techniques to separately verify the applied pressure, this *IC* metric would allow for measurement of the successful placement of engineered microbubbles for intra-treatment monitoring.

Acknowledgment

We thank Dr. Tom Matula (U.W.) for his helpful advice.

References

[1] K. Ramaswamy, V. Marx, D. Laser, T. Kenny, T. Chi, M. Bailey, M. D. Sorensen, R. H. Grubbs, and M. L. Stoller, "Targeted Microbubbles: a novel application for the treatment of kidney stones," BJU Int. Vol. 116, pp. 9-16, pp. 2015.

[2] Y.A. Pishchalnikov, W. Behnke-Parks, K. Maeda, T. Colonius, M. Mellema, M. Hopcroft, A. Luong, S. Wiener, M.L. Stoller, T. Kenny, and D.J. Laser, "Experimental observations and numerical modeling of lipid-shell microbubbles with calcium-adhering moieties for minimally-invasive treatment of urinary stones," Proc. Meet. Acoust. Vol. 35, 020008 (2019).

[3] Y. A. Pishchalnikov, W. M. Behnke-Parks, K. Schmidmayer, K. Maeda, T. Colonius, T. W. Kenny, and D. J. Laser, "High-speed video microscopy and numerical modeling of bubble dynamics near a surface of urinary stone," J. Acoust. Soc. Am. Vol. 146, No. 1, pp. 516-531, 2019.

[4] W.-S. Chen, T.J. Matula, A.A. Brayman, L.A. Crum, "A comparison of the fragmentation thresholds and inertial cavitation doses of different ultrasound contrast agents," J. Acoust. Soc. Am. Vol. 113, pp. 643–651, 2003.

[5] David G. Bell, Matthew A. Hopcroft, William M. Behnke-Parks, "High-Throughput, Semi-Autonomous Measurement of Cavitation-Mediated Material Breakage," arXiv:1812.05576, 2018.

[6] C.E. Brennen, "Cavitation and Bubble Dynamics" Cambridge University Press, Cambridge, 2013.

[7] M. Lokhandwalla, B. Sturtevant, "Fracture mechanics model of stone comminution in ESWL and implications for tissue damage," Phys. Med. Biol. Vol. 45, pp. 1923–1940, 2000.

[8] D. E. Kruse, K. W. Ferrara, "A New Imaging Strategy Using Wideband Transient Response of Ultrasound Contrast Agents," IEEE Trans Ultrasonics Ferroelectrics Freq Control. Vol. 52, No. 8, pp. 1320–1329, 2005.

[9] A. D. Maxwell, C. A. Cain, T. L. Hall, J. B. Fowlkes, Z. Xu, "Probability of Cavitation for Single Ultrasound Pulses Applied to Tissues and Tissue-Mimicking Materials," Ultrasound Med. Biol. Vol. 39, No. 3, Pages 449–465, 2013.

[10] N. de Jong, A. Bouakaz, and P. Frinking, "Basic Acoustic Properties of Microbubbles," Echocardiography, Vol. 19, No. 3, April 2002.

[11] E. Cramer and W. Lauterborn, "Acoustic cavitation noise spectra," Appl. Sci. Res. Vol. 38, pp. 209–214, 1982.

[12] V.I. Ilyichev, V. L. Koretz and N. P. Melnikov, "Spectral characteristics of acoustic cavitation," Ultrasonics Vol. 27, No. 6, pp. 357-361, 1989.